Interfacial interactions between local defects in amorphous SiO₂ and supported graphene

A. N. Rudenko,[1,*] F. J. Keil,[1] M. I. Katsnelson,[2] and A. I. Lichtenstein[3]

[1]*Institute of Chemical Reaction Engineering, Hamburg University of Technology, Eissendorfer Strasse 38, DE-21073 Hamburg, Germany*
[2]*Institute for Molecules and Materials, Radboud University Nijmegen, Heijendaalseweg 135, NL-6525 AJ Nijmegen, The Netherlands*
[3]*Institute of Theoretical Physics, University of Hamburg, Jungiusstrasse 9, DE-20355 Hamburg, Germany*

We present a density functional study of graphene adhesion on a realistic SiO₂ surface taking into account van der Waals (vdW) interactions. The SiO₂ substrate is modeled at the local scale by using two main types of surface defects, typical for amorphous silica: the oxygen dangling bond and three-coordinated silicon. The results show that the nature of adhesion between graphene and its substrate is qualitatively dependent on the surface defect type. In particular, the interaction between graphene and silicon-terminated SiO₂ originates exclusively from the vdW interaction, whereas the oxygen-terminated surface provides additional ionic contribution to the binding arising from interfacial charge transfer (*p*-type doping of graphene). Strong doping contrast for the different surface terminations provides a mechanism for the charge inhomogeneity of graphene on amorphous SiO₂ observed in experiments. We found that independent of the considered surface morphologies, the typical electronic structure of graphene in the vicinity of the Dirac point remains unaltered in contact with the SiO₂ substrate, which points to the absence of the covalent interactions between graphene and amorphous silica. The case of hydrogen-passivated SiO₂ surfaces is also examined. In this situation, the binding with graphene is practically independent of the type of surface defects and arises, as expected, from the vdW interactions. Finally, the interface distances obtained are shown to be in good agreement with recent experimental studies.

PACS number(s): 68.35.Np, 68.35.Dv, 73.22.Pr, 73.20.At

I. INTRODUCTION

Graphene, a single layer of graphite, is subject of intensive research owing to its remarkable electronic properties, which make this material a promising candidate for various electronic applications.[1–3] Since graphene is one-atom thick, its properties are strongly influenced by the environment, such as, for example, atomic impurities,[4] molecular adsorbates,[5] metallic contacts,[6,7] and dielectric substrates.[8,9] In respect to practical applications, the behavior of graphene in contact with substrates is of great importance. Since the discovery of graphene the role of substrates in its properties is actively debated, but is still not clearly understood.

Silicon dioxide is the main insulating component of present microelectronic devices owing to its perfect dielectric behavior and chemical stability.[10] However, this material is not the best candidate for its use as a substrate for graphene-based devices. In comparison to the remarkably high carrier mobility observed in suspended graphene,[11] carrier mobility in graphene supported on SiO₂ is very limited by scattering from surface states, by surface phonons, and by structural deformations of graphene.[12–14] The deformations are attributed not to intrinsic corrugations of graphene,[15,16] which might also exist in SiO₂-supported graphene,[17] but rather to the morphology of the SiO₂ surface itself, which is amorphous and, therefore highly disordered.[18] It has been demonstrated that the rippling of graphene can be considerably suppressed by its deposition on relatively flat surfaces, such as, for example, muscovite mica[14] or hexagonal boron nitride.[19] Furthermore, it has been shown that the adhesion of graphene on SiO₂ is essentially conformal, meaning that graphene reproduces the substrate topography with very high accuracy.[20] Apparently, interfacial interactions play a key role in the understanding of the structural behavior of graphene supported on surfaces. Nevertheless, the microscopic nature of the graphene adhesion on realistic SiO₂ has not yet been clearly established.

Apart from the structural changes of graphene, a substrate can directly affect its electronic properties by induced charges as shown by scanning tunneling microscopy (STM) experiments.[22] Furthermore, recent electrical field microscopy (EFM) experiments have demonstrated that the electrical potential of amorphous SiO₂ surface is rather disordered, which suggests the existence of localized chargelike impurities or surface defects.[23] The morphology of possible surface defects, their influence on the properties of graphene, and the bonding mechanisms in the graphene-substrate system are yet unclear from the theoretical point of view and require a detailed microscopic analysis.

So far, a number of papers reported theoretical first-principles investigations of graphene on SiO₂.[8,24–29] For modeling of the amorphous silica surface, various crystalline approximations are usually used paying not much attention to the structural peculiarities of realistic SiO₂. As a consequence, the results substantially differ from one approximation to another. For instance, the oxygen-terminated (001) surface of *α*-quartz was predicted to be very reactive,[24,25] significantly affecting the electronic properties of graphene, whereas the corresponding reconstructed surface is essentially inert and has no influence on the electronic structure of graphene.[28] Although the structure of amorphous SiO₂ is not trivial, it has only certain types of structural features (defects),[30,31] and thus could be rationally modeled only within the frame of specific crystalline approximations. In addition, previous investigations of graphene on SiO₂ do not explicitly consider dispersive interactions, but employ only local density approximations (LDA) for the treatment of exchange-correlation effects. Although the LDA interlayer distances are very close to experimental values for some layered materials (e.g., graphite),

this approximation is purely local and not able to describe dispersive interactions of nonlocal nature. As a consequence, it is impossible to reproduce accurately the binding energies and elastic properties of vdW complexes within the LDA. As has been shown, the dispersive interactions play a significant role in the adhesion of graphene on silicate surfaces.[9] For this reason, it is desirable to use more sophisticated approaches, allowing for explicit treatment of the vdW interactions.

In this paper we present a first-principles van der Waals density-functional study (vdW-DF) of graphene supported on amorphous SiO$_2$. Particularly, we are focused on the interaction between graphene and its substrate as well as on the electronic structure of supported graphene. We model the SiO$_2$ substrate by considering idealized surfaces with two main surface defects, typical for amorphous silica: the oxygen dangling bond and three-coordinated silicon. It is assumed that this structural model represents a realistic SiO$_2$ surface at the local scale. Additionally, we also examine the effect of hydrogen passivation of the surface defects considered. The account of the vdW interactions allowed us to estimate the vdW part of the graphene-SiO$_2$ interaction, which is found to be ranging from 23.8 to 39.6 meV/C depending on the particular surface type. In the case of hydrogen passivated surfaces as well as for the silicon-terminated surface, the vdW interactions play a dominant role. By contrast, for the oxygen-terminated surface, the vdW part is responsible only for half of the total binding energy. The rest arises from the charge transfer and from resulting ionic interactions between graphene and the underlying surface. In addition, we show that in the absence of interfacial covalent bonding with the substrate, the electronic structure of graphene remains virtually unaltered, which may play an important role for practical applications. Finally, calculated interlayer distances and obtained charge inhomogeneity for graphene on SiO$_2$ are found to be in agreement with the data of atomic force microscopy (AFM) and STM experiments,[18,22] respectively. This agreement justifies the structural model and computational approaches used in the present study.

The paper is organized as follows. In Sec. II, we briefly describe the methods of the investigation. In Sec. III, we present the structural model of the SiO$_2$ surface and describe other structural parameters used in our study. In Sec. IV A, we analyze the properties of the model SiO$_2$ surfaces. The results on interface geometry, adhesion, and electronic properties of graphene on SiO$_2$ are discussed in Secs. IV B, IV C, and IV D, respectively. Comparison with other theoretical studies are given in Sec. IV E. In the last section, we briefly summarize our results.

II. CALCULATION DETAILS

The results presented in this study have been obtained based on the plane-wave pseudopotential method as implemented in the QUANTUM-ESPRESSO simulation package.[32,33] To calculate adhesion energies and properly take into account dispersive interactions, exchange and correlation effects have been treated according to the vdW-DF method proposed by Dion *et al.*[34,35] Up to now, this method has been extensively applied to a large variety of compounds showing transferability across a broad spectrum of interactions, such as ionic, covalent, and vdW.[36] Although the vdW-DF method does not usually

provide chemical accuracy, it has distinct advantages over the standard (semi)local approximations, such as explicit inclusion of the nonlocal electron correlations, leading to the proper description of the dispersive interactions.

Within the vdW-DF, the exchange-correlation energy functional consists of several contributions,

$$E_{xc}(n) = E_x^{\text{revPBE}}(n) + E_c^{\text{LDA}}(n) + E_c^{\text{nl}}(n), \quad (1)$$

where the first term corresponds to the exchange part of the revised PBE (revPBE) functional,[37] E_c^{LDA} is the correlation energy within the LDA, and $E_c^{\text{nl}}(n)$ is the nonlocal correlation correction, which is calculated in the following way:

$$E_c^{\text{nl}} = \frac{1}{2} \int d^3r\, d^3r'\, n(r)\phi(r,r')n(r'), \quad (2)$$

where $n(r)$ is the electronic density and $\phi(r,r')$ is a function incorporating many-body density response (for details see Ref. 34). It should be emphasized that we evaluate the nonlocal correction [see Eq. (2)] in a perturbative way, i.e., using only GGA-based (semilocal) electronic density distribution. This choice looks quite reasonable since the vdW interactions are rather weak and thus cannot significantly change the electronic distribution. Moreover, as has been shown on different vdW complexes, the effects due to lack of self-consistency are negligible.[35] To calculate this correction to the total energy, we used an efficient post-processing routine NOLOCO from the EXCITING code.[41,42]

Self-consistent treatment of the dispersion effects within the vdW-DF approach is considerably more demanding in terms of the computational time. As a result, an efficient calculation of forces acting on atoms is also rather problematic for large systems. For this reason, we do not use straightforward geometry optimization of the graphene/SiO$_2$ system within the vdW-DF functional. Instead, we optimize only the isolated SiO$_2$ surfaces within the gradient corrected functional in the revised PBE parametrization.[37] This choice appears reasonable since the vdW interactions can be neglected for the energies of silica structures. Furthermore, we assume that the structure of graphene remains essentially unperturbed upon adhesion (see Sec. IV B for discussion). In order to find equilibrium separations between graphene and its substrates, we calculated adhesion energies as a function of the distance between them:

$$E_{\text{adh}}(d) = E_{\text{Gr+Surf}}(d) - E_{\text{Gr}} - E_{\text{Surf}}, \quad (3)$$

where $E_{\text{Gr+Surf}}(d)$ is the vdW-DF energy of graphene separated at the distance d from the surface, whereas E_{Gr} and E_{Surf} are the energies of noninteracting graphene and the surface, respectively. The minimum of the given function corresponds to the adhesion energy at the equilibrium separation, $\min[E_{\text{adh}}(d)] = E_{\text{adh}}(d_{\text{eq}})$.

In our calculations, we employed an energy cutoff of 30 Ry for the plane-wave basis and 300 Ry for the charge density. Self-consistent calculations of the Kohn-Sham equations were carried out employing the convergence criterion of 10^{-8} Ry. For accurate Brillouin-zone integration, the tetrahedron scheme[38] and a $(16 \times 16 \times 1)$ Monkhorst-Pack **k**-point mesh[39] were used. A much finer mesh $(48 \times 48 \times 1)$ and a Gaussian broadening of 0.01 Ry were used for the density of states (DOS) calculations. We checked that further increase of computational accuracy does not significantly change the

results. In all cases under consideration, the height of the supercell was chosen to be 50 Å. In order to avoid spurious interactions between images of the supercell in the [001] direction, we also used a dipole correction.[40] The convergence criterion for the relaxation of the SiO$_2$ surfaces was set to 0.001 Ry/Å. The positions of the lowermost layer of atoms were fixed.

III. SURFACE STRUCTURES

First-principles studies of amorphous compounds like SiO$_2$ are challenging due to lack of translational symmetry in these systems. In many cases the surface structure of amorphous SiO$_2$ is modeled using various crystalline approximations.[8,24–29,43–46] Specifically, various faces and terminations of α-quartz and β-cristobalite are frequently used to reproduce the structure of SiO$_2$. In this respect the structure of β-cristobalite seems to be more appropriate since β-cristobalite and amorphous SiO$_2$ have very similar local structures, as has been shown by neutron diffraction experiments.[47,48] However, in contrast to crystalline phases of SiO$_2$, the surface structure of the amorphous phase is nonuniform and has different reactive sites, which leads to unique chemistry of this surface.[49]

According to atomistic molecular dynamics simulations,[31] there are three types of stable point defects on amorphous SiO$_2$ surface: (i) O$_3$≡Si•, threefold coordinated silicon with no dangling oxygen bonds (Q_3^0), (ii) O$_3$≡Si−O•, fourfold coordinated silicon with one dangling oxygen bond (Q_4^1), and (iii) threefold coordinated silicon with one dangling oxygen bond (Q_3^1). The notation Q_m^n here implies m-coordinated silicon with n oxygen dangling bonds. For convenience, we will use this notation throughout the paper. Moreover, as follows from the atomistic simulations, Q_3^0 and Q_4^1 are the most common defect sites ($\sim$80% of the total surface area), which is in agreement with other theoretical investigations.[30] From the experimental point of view these two defect types also can be considered as fundamental in amorphous SiO$_2$.[50] An additional important type of chemical environment for silica is Q_4^0, which corresponds to bulk silica without defects and can be also modeled as a passivated surface defect (e.g., by hydrogen). In practice, partial passivation of the SiO$_2$ surface can be achieved by exposure to molecular hydrogen (H$_2$) even at room temperatures.[50] In principle, the emergence of other surface defects is possible, but their existence is energetically unfavorable and, with high probability, leads to a local reconstruction of the surface. Interestingly, the reconstructed surface of crystalline α-quartz phase is predicted to be fully saturated owing to the formation of six-membered rings at the surface.[51,52] This is, however, a consequence of the long-range order of crystalline surfaces and is not likely to occur for amorphous surfaces.

Unsaturated surfaces are usually reactive and easily adsorb impurities from the environment to passivate themselves. Such a passivation can be, in principle, avoided under ultrahigh vacuum (UHV) conditions. However, as has been previously demonstrated by EFM experiments, the amorphous SiO$_2$ surface shows relatively large fluctuations of electrical potential at ambient conditions.[23] This fluctuations suggest the existence of uncompensated surface charges even without UHV, which can be associated with unsaturated surface defects.
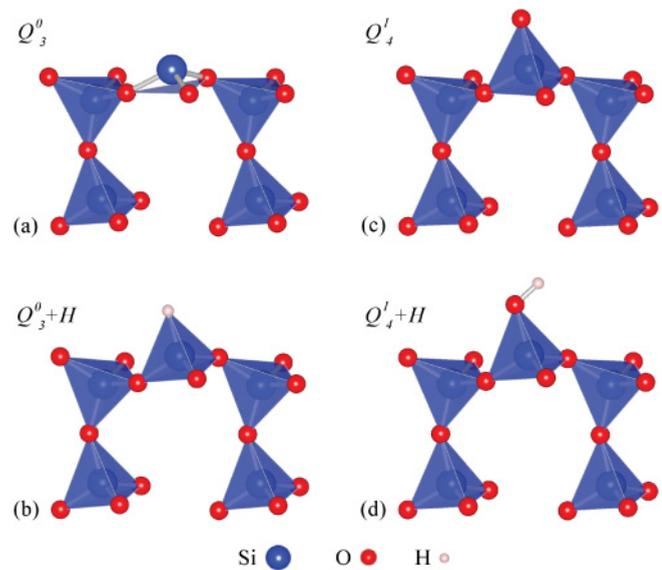
FIG. 1. (Color online) Surface structures of SiO$_2$ with the main types of defects (side view): (a) threefold coordinated silicon, Q_3^0, (b) Q_3^0 terminated by hydrogen atom, (c) single oxygen dangling bond, Q_4^1, and (d) Q_4^1 terminated by hydrogen atom.

We believe that the chemical reactivity of realistic amorphous silica can be defined by a certain combination between the reactivities of local surface regions. This regions can be modeled by idealized surfaces, each of which contains only one defect type among those discussed above. In turn, the properties of graphene at a large scale (realistic SiO$_2$) are expected to be composed of its properties at the local scale (idealized SiO$_2$). Besides computational advantages within the first-principles framework, this approach allows us to investigate the role of different surface defects separately. In our work, for modeling the SiO$_2$ surface, we consider two different β-cristobalite surfaces with morphologies corresponding to the Q_3^0 and Q_4^1 defect sites. We show relaxed structures of these surfaces in Figs. 1(a) and 1(c). As we already mentioned, these two defects are the most numerous types in amorphous SiO$_2$ according to the previous studies.[30,31] We do not consider the Q_3^1 defect mainly because it would have been necessary to consider a (100) surface of β-cristobalite instead of a (111) surface that is suitable for the modeling of Q_3^0 and Q_4^1-defective surfaces. However, the unit cell of a (100) β-cristobalite surface is not commensurate with the unit cell of graphene in lateral directions. In this case, the lattice constant mismatch is more than 10% and the corresponding adjustment of the SiO$_2$ unit cell would considerably affect the properties of the surface. Since the Q_3^1 defect contains one oxygen dangling bond and one three-coordinated silicon, it is reasonable to suppose that this defect type may be approximated by two separated defects, Q_4^1 and Q_3^0. In addition to unsaturated surfaces, we investigate the effect of hydrogen passivation on adhesive properties of SiO$_2$ surfaces [see Figs. 1(b) and 1(d)]. In Fig. 2, we show schematically the structure of graphene supported on SiO$_2$ with various defects on its surface.

In all cases, the supercell used in our study contains three layers of defectless (SiO$_4$)$^{4-}$ tetrahedra and one topmost defective layer. Oxygen atoms in the lowermost layer are
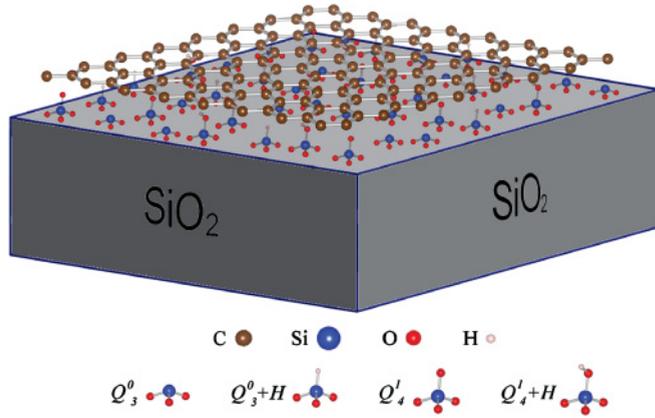
FIG. 2. (Color online) Schematic representation of graphene supported on a SiO_2 surface with different defects on the top (according to the model employing in this work).

saturated by hydrogen atoms. All atoms except the lowermost layer of hydrogen were relaxed. We used lateral $(2 \times 2)a$ graphene unit-cell parameters for the SiO_2-graphene supercell, which corresponds to a $\sim3\%$ laterally compressed (111) surface unit cell of β-cristobalite.[53] We believe this choice is justified since silicates are known to have a relative low bulk moduli, i.e., they can be compressed quite easily.[54]

As for graphene, it has a two-dimensional honeycomb lattice of sp^2-bonded carbon atoms. Although the real structure of graphene is corrugated, the characteristic length of corresponding ripples is around 100 Å,[15,16] which is much larger than the typical length of supercells used in first-principles calculations. For this reason, we do not consider this phenomenon in our work. We used a lattice constant of graphene equal to $a = 2.459$ Å in accordance with the experimentally obtained value for graphite at low temperatures.[55]

IV. RESULTS AND DISCUSSION

A. Bare SiO_2 surfaces

In Fig. 3, we show densities of electronic states for the SiO_2 surfaces under investigation. One can see that the H-passivated surfaces [see Figs. 3(b) and 3(d)] are fully saturated and there are no resonances within the band gap, indicating the absence of localized states at the surface. In these cases, the DOS exhibits a band gap of ~5.7 eV, which is comparable with the band gap of bulk β-cristobalite calculated using the PBE functional (5.84 eV).[56] These values, however, underestimate the experimental gap of amorphous SiO_2 films (9.3 eV),[57] which is related to the well-known problem of the standard density functional theory (DFT) functionals (LDA/GGA), such as inability to accurately describe electronic spectra for compounds with strong electron localization. The band gap of silica can be considerably improved using hybrid functionals (e.g., PBE0[58] or GW approximation.[59] In our work, however, we are not focused on a precise quantitative description of the electronic properties of SiO_2. We believe that the use of more appropriate approaches will not qualitatively affect the results obtained in this study.

In contrast to H-passivated SiO_2, defective surfaces are unsaturated and, therefore the DOS exhibits resonances within
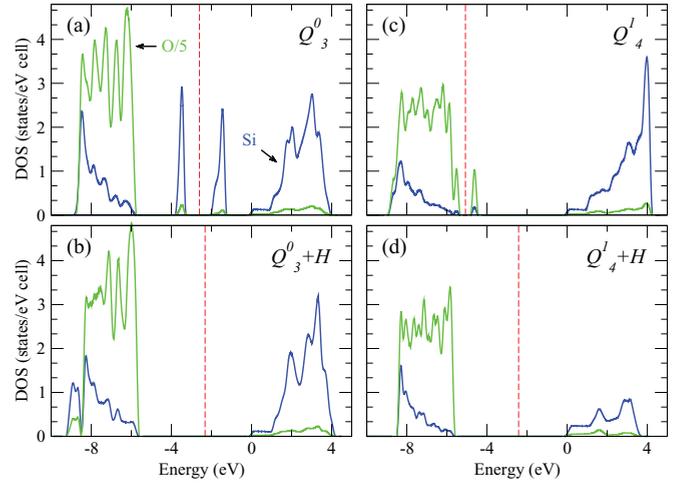
FIG. 3. (Color online) Densities of states for SiO_2 surfaces projected onto Si (blue line) and O (green line) atoms: (a) and (c) surfaces covered by the Q_3^0 and Q_4^1 defects, respectively; (b) and (d) corresponding hydrogen-passivated surfaces. Oxygen DOS is reduced by a factor of five for clarity. The vertical line corresponds to the Fermi level. Zero energy coincides with the lower energy of the conduction band.

the band gap arising from the localized surface states. For each surface, there are two peaks corresponding to occupied and unoccupied states of opposite spin. In the case of surface with undercoordinated silicon (the Q_3^0 defect), the midgap states originate from the $Si(3s,3p)$ and $O(2p)$ orbitals, whereas for the Q_4^1 defect the resonance is slightly more intense and localized mainly at the $O(2p)$ orbital. The presence of localized surface states allows one to expect chemisorption of graphene on a surface. Indeed, with respect to graphene supported on SiO_2, the defect sites may be effectively considered as monovalent impurities. In turn, such impurities may bind ionically or covalently with graphene.[4]

In order to estimate chemical activity of the surfaces in respect to graphene, we calculate the work functions (WF) and electron affinities (EA) as $(E_{vac}$-$E_F)$ and $(E_{vac}$-$E_{cond})$, respectively, where E_{vac} is the vacuum level of the electrostatic potential, E_F is the Fermi level, and E_{cond} is the lowest energy of the conduction band. We stress, however, that the accuracy of the WF and EA is limited within the employed computational method, similar to the band-gap problem (see above). Nevertheless, these quantities are useful to establish general trends in the chemisorption of graphene on SiO_2. In Table I, we summarize calculated WF and EA for SiO_2 surfaces and graphene. For graphene, WF is equal to EA due to the absence of a band gap. Comparing WF and EA for graphene and H-passivated surfaces, one can see that the surface WF is larger than the EA of graphene (and vice versa). The same situation occurs for graphene and the surface with the Q_3^0 defects. This implies that the charge transfer between these surfaces is not energetically favorable. On the other hand, the WF of graphene is lower than the EA of the surface with oxygen dangling bond (Q_4^1), which suggests electronic transfer from graphene toward this surface (p-type doping of graphene).

TABLE I. Work functions (WF) and electron affinities (EA) calculated for different SiO_2 surfaces (see Sec. III for details) and graphene.

	Q_3^0	$Q_3^0 + H$	Q_4^1	$Q_4^1 + H$	graphene
WF, eV	5.6	8.0	9.3	7.2	4.2
EA, eV	4.1	2.3	8.6	1.6	4.2

B. Geometry of the graphene-SiO$_2$ interface

As we already mentioned in Sec. II, we calculate equilibrium graphene-SiO$_2$ distances assuming that the structure of graphene is unperturbed upon contact with the substrate. However, this does not reflect the structure of graphene on SiO$_2$ on a large scale. As follows from experimental studies, the structure of graphene supported on amorphous SiO$_2$ is highly corrugated owing to high-fidelity conformation.[17,18,20] The assumed invariability of graphene is resulting from the employed theoretical approach. Indeed, the supercell used in our study is too small in lateral directions to reveal corrugations of graphene caused by the irregularity of the substrate. Moreover, imposed boundary conditions along with the strong sp^2 bonding of carbon atoms artificially restrict the flexibility of graphene. Previous results show that for such small supercells the deformation of graphene is really negligible.[9] Thus we note that our results reflect only the local behavior of graphene on SiO$_2$. Therefore the interlayer distance is the main structural parameter in our model. In Table II, we summarize these parameters for different SiO$_2$ surfaces.

Equilibrium distances between graphene and SiO$_2$ are considerably different for the surfaces covered by the Q_3^0 and Q_4^1 defects. This can be easily accounted for by noticing that the difference in the distance correlates with the difference in the adhesion energy. Namely, the smaller distance corresponds to the larger E_{adh} and vice versa. The situation for hydrogen-passivated defects is different. In this case, although the binding energy is smaller relative to the binding for the Q_3^0 defect, the interlayer distance is also smaller. This is caused by the fact that the orbitals associated with hydrogen have a small

TABLE II. Calculated interlayer distances, adhesion energies, Fermi level shifts, and WFs (EAs) for graphene supported on different SiO$_2$ surfaces. Interlayer distances are calculated as a difference between the z coordinate of carbon atoms in graphene and the topmost atomic layer of the substrate. The Fermi level shift implies the difference between the Dirac point and the Fermi level of supported graphene. The values are given for the most stable graphene geometry.

	Q_3^0	$Q_3^0 + H$	Q_4^1	$Q_4^1 + H$
d_{eq}, Å	3.6	2.7	2.7	2.6
E_{adh}, meV/C	−31.6	−26.5	−77.7	−24.8
vdW part of E_{adh}[1]	98%	96%	51%	96%
ΔE_F, eV	0.0	0.0	−1.0	0.0
WF (EA), eV	4.2	4.2	5.2	4.2

[1]Contribution of vdW interaction calculated as a difference between adhesion energies in the presence of nonlocal correlations and without it.

spread, i.e., they are not much spatially extended compared to the oxygen or silicon orbitals. As a consequence, the Pauli repulsion between graphene and the hydrogen layer decreases more rapidly with distance, which allows graphene to come closer to hydrogen.

The interface distances obtained between graphene and SiO$_2$ can be compared with experimental height histograms acquired across the graphene-SiO$_2$ boundary using the AFM technique.[18] According to the experimental data, the average thickness of a single graphene layer deposited on SiO$_2$ under UHV conditions can be estimated as 4.2 Å. This quantity, however, does not reflect the actual distance of the interface since it directly depends on the spatial extension of the orbitals of both surfaces. In fact, the π orbitals of graphene are known to have a rather large spread (see, e.g., Ref. 60) and, therefore, the thickness of graphene supported on a surface with more localized orbitals should be larger than the distance in the theoretical sense, i.e., as a difference between atomic coordinates. On the other hand, if the thickness of the topmost atomic layer is *much* smaller than the thickness of supported graphene, the interlayer distance corresponds to half of the graphene thickness. It is difficult to establish a more precise relationship between these quantities because of a number of ambiguities in the determination of the orbital spread and its quantitative influence on experimental results. According to this consideration, the average experimental distance should satisfy the following uncertainty relation: $h/2 < d_{exp} < h$, where h is the average experimental thickness. Thus, for the mentioned experiment,[18] the distance d_{exp} is bounded within 2.1–4.2 Å. One can see that obtained theoretical distances calculated according to the given structural model of the SiO$_2$ surface (see Table II) fall entirely within this range. Taking the uncertainty into account, we come to a good agreement between results obtained and experimental estimations. It should be noted that the obtained distances are rather sensitive to the presence of the vdW interactions, especially if they dominate. In fact, the distances calculated without the nonlocal term in the exchange-correlation functional [see Eq. (2)] are significantly higher and therefore do not lead to an agreement with the experiment.

C. Graphene adhesion on SiO$_2$

As follows from Table II, the main contribution (96%) to adhesion of graphene on H-passivated SiO$_2$ surfaces comes from the vdW interaction. Adhesion energies for $Q_3^0 + H$ and $Q_4^1 + H$ cases are very close to each other, which indicates that the vdW part of the adhesion energy is only slightly dependent on the particular surface type. The situation for unsaturated surfaces is partially different. In the case of a surface with undercoordinated silicon (Q_3^0), the vdW contribution still dominates (98%) leading to the adhesion energy that is slightly larger than for the H-passivated case, whereas the presence of dangling oxygen bonds on the surface (Q_4^1) results in a much stronger adhesion of only 51% of the vdW interaction. The latter implies that graphene definitely chemisorbs on the surface with Q_4^1 defect, which is the most reactive among the others. The values in Table II are given for the most stable configuration of graphene relative to the considered surfaces. Namely, for all considered surface defects, this configuration

corresponds to the situation where point defects are situated below a hollow (hexagon center) graphene site. If the defect is located below a bridge (center of the C-C bond) or top site (C atom), the maximum difference in adsorption energy is reached for the oxygen terminated surface ($\sim$5 meV/C). For three other surfaces considered, this difference is not exceeding 1 meV/C. It is worth mentioning that irrespective of the surface type, values obtained for the adhesion energies are sufficiently exceeding the elastic energy stored in graphene ($\sim$0.8–2.6 meV/C).[18,20] This means that the interaction energy between graphene and SiO_2 is large enough to overcome the energy needed for graphene to follow the SiO_2 morphology. Therefore, our results confirm previous estimations regarding the possibility of graphene-SiO_2 conformation.

Very recently, the first direct measurements of the adhesion energy of 1–5 layer graphene to SiO_2 were reported.[21] For monolayer graphene the value of 0.45 ± 0.02 J/m^2 ($\sim 74 \pm 3$ meV/C) was obtained. As can be seen, the experimental adhesion energy is very close to our theoretical estimation (77.7 meV/C) for the oxygen-terminated surface (Q_4^1 defect), but significantly higher than for the other surface types. This might imply that the Q_4^1 defect is the most common defect at the SiO_2 surface in the experiment. However, in view of the fact that the Q_4^1 defect can be considered as a charge impurity (as we show below), this assumption seems to be inconsistent with the reported expectations that charge impurities should not significantly affect the adhesion because of their relatively low density in SiO_2. We believe that in order to resolve this contradiction, a more reliable large-scale model for the SiO_2 structure is required, where concentration and distribution of the (sub)surface defects are explicitly taken into account. We leave this problem open for further studies.

D. Electronic structure and charge transfer in supported graphene

In Fig. 4, we show DOS for graphene on SiO_2. As there is no chemisorption between graphene and H-passivated SiO_2 surfaces, the electronic structure of these systems is not changing upon adhesion [see Figs. 4(b) and 4(d)]. In this situation, the Dirac point of graphene coincides with the Fermi level and lies in the center of the substrate band gap. The same is true for the Q_3^0-defective surface with the exception that the DOS of graphene is slightly distorted in the vicinity of impurity resonances. This may indicate a slight orbital hybridization between graphene and the surface. However, these distortions are small enough to produce any noticeable changes in the adhesion energy. As we have shown before, in the case of graphene adherent to the Q_4^1 surface, there should be additional sources of the interaction apart from the vdW one. Namely, as follows from Table I, p-type doping of graphene is expected since the EA of the Q_4^1 surface is larger than the WF of isolated graphene. This is also clear from the DOS [see Fig. 4(c)] that exhibits the Fermi level shift toward the low-energy range relative to the Dirac point. Such a shift means that graphene works as a donor on the Q_4^1-defective SiO_2 surface. As can be also seen in Fig. 4(c), the Fermi level lies at the impurity resonance suggesting that the electrons from graphene are transferred to the p-orbital of oxygen, which becomes partially occupied. Löwdin charge analysis[61] shows the charge doping of 0.29 e^-/cell.
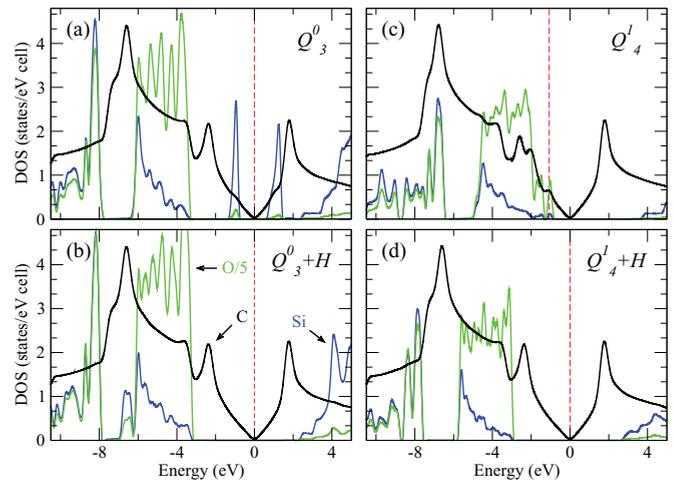
FIG. 4. (Color online) Densities of states of SiO_2 surfaces in contact with graphene sheet projected onto C (black line), Si (blue line), and O (green line) atoms. The SiO_2 substrates are given in the same order as in Fig. 3. Oxygen DOS is reduced by a factor of five. The vertical line corresponds to the Fermi level. Zero energy coincides with the Dirac point of graphene.

The Fermi level shift implies the existence of induced charges in local regions of supported graphene, which can be considered as Coulomb impurities. This finding is in agreement with experimental STM studies, where electron-density inhomogeneities have been clearly observed in graphene flakes placed on a SiO_2 substrate.[22] Raman spectroscopy studies also provide some evidences for the p-type doping of graphene on SiO_2.[62] Our results allow one to identify more specifically the origin of the charge inhomogeneities and associate them with the Q_4^1 surface defect. The presence of these impurities plays a significant role for charge-carrier scattering and may affect the electron mobility of a sample. This is especially important for graphene supported on a SiO_2 substrate, where mobility is considerably limited in comparison to suspended graphene.[12] Although there are a number of sources restricting the mobility of graphene, charged impurities seem to be one of the dominating factors, at least at low temperatures.[13] It is interesting to note that the overall mobility of graphene depends on the distribution of the charged impurities on its surface.[63,64] In particular, the contribution of impurities to the resistivity is maximal for their homogeneous distribution and can be strongly suppressed by clusterization. In the case under investigation, these effects depend on the particular SiO_2 morphology.

Apart from the Fermi level shift indicating the charge transfer from graphene to the Q_4^1 surface, there is a distortion of the graphene DOS within the energy range of -3 to 1 eV relative to the Dirac point. It is worth mentioning that no distortions occur in the vicinity of the Dirac point of graphene. The alteration of the DOS reflects some hybridization between the π orbitals of graphene and p orbitals of oxygen from the defective layer of SiO_2. Since the oxygen atom has only one unsaturated electron in the Q_4^1 defect, this defect site can be considered as a monovalent impurity in respect to graphene. According to Ref. 4, monovalent adsorbates on graphene can be divided into two separate groups regarding the bonding mechanism: ionically and covalently bonded

impurities. The main qualitative difference between these two groups is that the second type of impurities induces a band gap and corresponding midgap states at the Fermi level, whereas the first type gives rise only to impurity states lying below (or above) the Dirac point. Importantly, the typical band structure of graphene is preserved for ionic group of impurities. In accordance with this classification, the Q_4^1 defect site corresponds to an ionic impurity since it does not disturb significantly the band structure of graphene. We note that no qualitative changes in terms of the total DOS have been found among the different surface geometries of graphene.

Besides the covalent bonding, there is another mechanism of the band-gap opening in graphene, resulting from the symmetry breaking. If a binding partner interacts with one sublattice of graphene more strongly than with another sublattice, the graphene sublattice symmetry is broken, resulting in the band-gap opening. One of the prominent examples exhibiting this effect is graphene supported on the surface of hexagonal boron nitride.[66] For graphene supported on the SiO$_2$ surfaces, we also found this effect, however, in all cases considered the interaction between graphene and its substrate is relatively weak and the band gap is not exceeding 15 meV. Since this value is less than the thermal energy at room temperature ($\sim$25 meV), we believe that this gap can be considered as negligible.

In Table II, we also give WFs of supported graphene. Since the substrate does not induce a band gap in graphene, its WFs coincide with EAs, as for isolated graphene. One can see that for all considered substrates, with the exception of the oxygen-terminated SiO$_2$ surface, the WF of supported graphene is equal to the WF of isolated graphene. This is a consequence of the absence of the chemical bonding between graphene and these surfaces. The WF (EA) of graphene on the surface with Q_4^1 defects is larger by the value of the Fermi level shift caused by the charge transfer. On a large scale, this means that the graphene sheet deposited on amorphous SiO$_2$ should possess unequal reactivity for different surface regions. This property might find application in practice as a novel graphene-based method for microscopic surface studies, along with existing ones.[65]

E. Comparison with other theoretical studies

Our results, in particular concerning the oxygen-terminated surface (Q_4^1 defect), might appear qualitatively inconsistent with previous DFT investigations of graphene on SiO$_2$ surfaces.[24,25,29] In these works, an evident covalent bonding has been observed between graphene and SiO$_2$ along with significant structural reconstruction both of graphene and the surface. Moreover, according to these investigations the electronic structure of graphene undergoes significant modification upon contact with SiO$_2$. Considerable band-gap opening is also reported. It should be noted that the results mentioned have been obtained using the structure of α-quartz for modeling the SiO$_2$ surface. This means that a cut of this structure in the [001] direction corresponds to a surface with two oxygen dangling bonds per unit cell or, in other words, to a Q_4^2-defective surface. In contrast, our results for the oxygen-terminated surface have been obtained using the surface with only one oxygen dangling bond (Q_4^1 defect) per unit cell. Therefore, the mentioned inconsistency is not surprising since the Q_4^2 defect

is apparently more reactive than the Q_4^1. This is also consistent with Ref. 27 where no strong binding with graphene has been found in the case of Q_4^1-like surface termination. As we already stated in Sec. III, the existence of free-standing surface configuration like Q_4^2 is not energetically favorable and most probably would lead to a local reconstruction. Interestingly, if graphene is supported on a fully reconstructed SiO$_2$ surface,[28] neither covalent nor ionic interfacial interactions occur, which means that graphene physisorbs on the surface. The qualitative difference in the properties of graphene on various SiO$_2$ surfaces accentuates the importance of the realistic surface morphology in the determination of graphene properties. The results of electronic structure calculations for the hydrogenated surfaces considered in our work are in qualitative agreement with the mentioned investigations. Additionally, we note that the previous results were mainly obtained using the LDA functionals and, therefore, some quantitative discrepancies (e.g., in binding energies or interface distances) are legitimate.

V. CONCLUSION

We have investigated the nature of interfacial interactions between graphene and amorphous SiO$_2$ from first principles. We modeled SiO$_2$ surface assuming the existence of certain types of surface defects that are relevant for amorphous silica surface. Particularly, idealized surfaces with the oxygen dangling bond and three-coordinated silicon defects are considered, as well as the case of their hydrogen passivation. We found that the vdW interaction plays a dominant role in the adhesion of graphene on silicon- and hydrogen-terminated surfaces. This confirms the importance of the dispersive interactions for graphene supported on surfaces and also justifies the use of the nonlocal vdW correction. For the surface with dangling oxygen bonds, we found, apart from the vdW, an additional ionic contribution to the graphene-SiO$_2$ binding resulting from the electron transfer from graphene to the more electronegative SiO$_2$ surface. This contribution is responsible for half of the total binding energy.

We found that the DOS of supported graphene remains almost unperturbed retaining its typical Dirac shape. As a consequence, there is no covalent bonding between graphene and the surfaces considered. The only change in the electronic structure of graphene concerns the Fermi level shift for the oxygen-terminated substrate. This shift, caused by the Q_4^1 defect, implies the existence of charged impurities and may be partially responsible for the known transport anomalies of graphene on SiO$_2$.

Our results show that different surface terminations lead to the variations of the distances between graphene and SiO$_2$. Unfortunately, these variations cannot be directly related to experimental observations due to the complexity of the realistic SiO$_2$ morphology. Nevertheless, obtained interface distances are comparable with the average thickness of supported graphene observed in AFM experiments. This thickness allows us to estimate the average graphene-SiO$_2$ distance. Taking into account ambiguities in the accurate determination of this distance, our theoretical results agree well with experimental data. This agreement shows the rationality of the structural model for amorphous SiO$_2$ used in our study.

*rudenko@tu-harburg.de

[1] K. S. Novoselov, A. K. Geim, S. V. Morozov, D. Jiang, Y. Zhang, S. V. Dubonos, I. V. Grigorieva, and A. A. Firsov, Science **306**, 666 (2004).

[2] A. K. Geim and K. S. Novoselov, Nat. Mater. **6**, 183 (2007).

[3] A. H. Castro Neto, F. Guinea, N. M. R. Peres, K. S. Novoselov, and A. K. Geim, Rev. Mod. Phys. **81**, 109 (2009).

[4] T. O. Wehling, M. I. Katsnelson, and A. I. Lichtenstein, Phys. Rev. B **80**, 085428 (2009).

[5] A. N. Rudenko, F. J. Keil, M. I. Katsnelson, and A. I. Lichtenstein, Phys. Rev. B **82**, 035427 (2010).

[6] P. A. Khomyakov, G. Giovannetti, P. C. Rusu, G. Brocks, J. van den Brink, and P. J. Kelly, Phys. Rev. B **79**, 195425 (2009).

[7] I. Hamada and M. Otani, Phys. Rev. B **82**, 153412 (2010).

[8] T. O. Wehling, A. I. Lichtenstein, and M. I. Katsnelson, Appl. Phys. Lett. **93**, 202110 (2009).

[9] A. N. Rudenko, F. J. Keil, M. I. Katsnelson, and A. I. Lichtenstein, Phys. Rev. B **83**, 045409 (2011).

[10] M. Itsumi, *SiO₂ in Si Microdevices*, (Kodansha, Tokyo/Springer, Berlin, 2002).

[11] K. I. Bolotin, K. J. Sikes, Z. Jiang, M. Klima, G. Fudenberg, J. Hone, P. Kim, and H. L. Stormer, Solid State Commun. **146**, 351 (2008).

[12] J.-H. Chen, C. Jang, S. Xiao, M. Ishigami, and M. S. Fuhrer, Nat. Nanotechnology **3**, 206 (2008).

[13] J.-H. Chen, C. Jang, M. Ishigami, S. Xiao, E. D. Williams, and M. S. Fuhrer, Solid State Commun. **149**, 1080 (2009).

[14] C. H. Lui, L. Liu, K. F. Mak, G. W. Flynn, and T. F. Heinz, Nature (London) **462**, 339 (2009).

[15] J. C. Meyer, A. K. Geim, M. I. Katsnelson, K. S. Novoselov, T. J. Booth, and S. Roth, Nature (London) **446**, 60 (2007).

[16] A. Fasolino, J. H. Los, and M. I. Katsnelson, Nat. Mater. **6**, 858 (2007).

[17] V. Geringer, M. Liebmann, T. Echtermeyer, S. Runte, M. Schmidt, R. Rückamp, M. C. Lemme, and M. Morgenstern, Phys. Rev. Lett. **102**, 076102 (2009).

[18] M. Ishigami, J. H. Chen, W. G. Cullen, M. S. Fuhrer, and E. D. Williams, Nano Lett. **7**, 1643 (2007).

[19] C. R. Dean, A. F. Young, I. Meric, C. Lee, L. Wang, S. Sorgenfrei, K. Watanabe, T. Taniguchi, P. Kim, K. L. Shepard, and J. Hone, Nat. Nanotechnology **5**, 722 (2010).

[20] W. G. Cullen, M. Yamamoto, K. M. Burson, J. H. Chen, C. Jang, L. Li, M. S. Fuhrer, and E. D. Williams, Phys. Rev. Lett. **105**, 215504 (2010).

[21] S. P. Koenig, N. G. Boddeti, M. L. Dunn, and J. S. Bunch, Nature Nanotechnology, doi:10.1038/nnano.2011.123.

[22] Y. Zhang, V. W. Brar, C. Girit, A. Zettl, and M. F. Crommie, Nat. Phys. **5**, 722 (2009).

[23] N. García, Z. Yan, A. Ballestar, J. Barzola Quiquia, F. Bern, and P. Esquinazi, J. Phys. Condens. Matter **22**, 045002 (2010).

[24] Y.-J. Kang, J. Kang, and K. J. Chang, Phys. Rev. B **78**, 115404 (2008).

[25] P. Shemella and S. K. Nayak, Appl. Phys. Lett. **94**, 032101 (2009).

[26] D. Li, W. Windl, and N. P. Padture, Adv. Mater. **21**, 1243 (2009).

[27] M. Z. Hossain, Appl. Phys. Lett. **95**, 143125 (2009).

[28] N. T. Cuong, M. Otani, and S. Okada, Phys. Rev. Lett. **106**, 106801 (2011).

[29] P. Jadaun, S. K. Banerjee, L. F. Register, and B. Sahu, e-print arXiv:1102.2557v1 (unpublished).

[30] B. P. Feuston and S. H. Garofalini, J. Chem. Phys. **91**, 564 (1989).

[31] M. Wilson and T. R. Walsh, J. Chem. Phys. **113**, 9180 (2000).

[32] P. Giannozzi, S. Baroni, N. Bonini, M. Calandra, R. Car, C. Cavazzoni, D. Ceresoli, G. L. Chiarotti, M. Cococcioni, I. Dabo, A. Dal Corso, S. de Gironcoli, S. Fabris, G. Fratesi, R. Gebauer, U. Gerstmann, C. Gougoussis, A. Kokalj, M. Lazzeri, L. Martin-Samos, N. Marzari, F. Mauri, R. Mazzarello, S. Paolini, A. Pasquarello, L. Paulatto, C. Sbraccia, S. Scandolo, G. Sclauzero, A. P. Seitsonen, A. Smogunov, P. Umari, and R. M. Wentzcovitch, J. Phys. Condens. Matter **21**, 395502 (2009).

[33] The pseudopotentials used in this work were taken from QUANTUM-ESPRESSO web page [http://www.quantum-espresso.org].

[34] M. Dion, H. Rydberg, E. Schröder, D. C. Langreth, and B. I. Lundqvist, Phys. Rev. Lett. **92**, 246401 (2004).

[35] T. Thonhauser, V. R. Cooper, S. Li, A. Puzder, P. Hyldgaard, and D. C. Langreth, Phys. Rev. B **76**, 125112 (2007).

[36] D. C. Langreth, B. I. Lundqvist, S. D. Chakarova-Käck, V. R. Cooper, M. Dion, P. Hyldgaard, A. Kelkkannen, J. Kleis, Lingzhu Kong, Shen Li, P. G. Moses, E. Murray, A. Puzder, H. Rydberg, E. Schröder, and T. Thonhauser, J. Phys. Condens. Matter **21**, 084203 (2009).

[37] Y. Zhang and W. Yang, Phys. Rev. Lett. **80**, 890 (1998).

[38] P. E. Blöchl, O. Jepsen, and O. K. Andersen, Phys. Rev. B **49**, 16223 (1994).

[39] H. J. Monkhorst and J. D. Pack, Phys. Rev. B **13**, 5188 (1976).

[40] L. Bengtsson, Phys. Rev. B **59**, 12301 (1999).

[41] D. Nabok, P. Puschnig, and C. Ambrosch-Draxl, Comput. Phys. Commun. **182**, 1657 (2011).

[42] [http://exciting-code.org].

[43] F. Vigné-Maeder and P. Sautet, J. Phys. Chem. B **101**, 8197 (1997).

[44] D. Ceresoli, M. Bernasconi, S. Iarlori, M. Parrinello, and E. Tosatti, Phys. Rev. Lett. **84**, 3887 (2000).

[45] D. Ricci and G. Pacchioni, Phys. Rev. B **69**, 161307 (2004).

[46] D. E. Jiang and E. A. Carter, Phys. Rev. B **72**, 165410 (2005).

[47] I. P. Swainson and M. T. Dove, Phys. Rev. Lett. **71**, 193 (1993).

[48] M. G. Tucker, M. P. Squires, M. T. Dove, and D. A. Keen, J. Phys. Condens. Matter **13**, 403 (2001).

[49] T. R. Walsh, M. Wilson, and A. P. Sutton, J. Chem. Phys. **113**, 9191 (2000).

[50] F. Messina and M. Cannas, J. Phys. Chem. C **111**, 6663 (2007).

[51] G.-M. Rignanese, A. De Vita, J.-C. Charlier, X. Gonze, and R. Car, Phys. Rev. B **61**, 13250 (2000).

[52]T. P. M. Goumans, A. Wander, W. A. Brown, and C. R. A. Catlow, Phys. Chem. Chem. Phys. **9**, 2146 (2007).

[53]F. Liu, S. H. Garofalini, R. D. King-Smith, and D. Vanderbilt, Phys. Rev. Lett. **70**, 2750 (1993).

[54]J. D. Bass, in *Mineral Physics and Crystallography: A Handbook of Physical Constants*, edited by T. J. Ahrens (American Geophysical Union, Washington, DC, 1995), p. 45.

[55]Y. Baskin and L. Meyer, Phys. Rev. **100**, 544 (1955).

[56]M. Luppi and S. Ossicini, Phys. Status Solidi A **197**, 251 (2003).

[57]Z. A. Weinberg, G. W. Rubloff, and E. Bassous, Phys. Rev. B **19**, 3107 (1979).

[58]A. Alkauskas and A. Pasquarello, Physica B **401–402**, 546 (2007).

[59]L. E. Ramos, J. Furthmüller, and F. Bechstedt, Phys. Rev. B **69**, 085102 (2004).

[60]F. Freimuth, Y. Mokrousov, D. Wortmann, S. Heinze, and S. Blügel, Phys. Rev. B **78**, 035120 (2008).

[61]P. O. Löwdin, J. Chem. Phys. **18**, 365 (1950).

[62]S. Ryu, L. Liu, S. Berciaud, Y. J. Yu, H. Liu, P. Kim, G. W. Flynn, and L. E. Brus, Nano Lett. **10**, 4944 (2010).

[63]M. I. Katsnelson, F. Guinea, and A. K. Geim, Phys. Rev. B **79**, 195426 (2009).

[64]K. M. McCreary, K. Pi, A. G. Swartz, Wei Han, W. Bao, C. N. Lau, F. Guinea, M. I. Katsnelson, and R. K. Kawakami, Phys. Rev. B **81**, 115453 (2010).

[65]M. I. Katsnelson, Science **329**, 1157 (2010); K. Xu, P. Cao, and J. R. Heath, *ibid*. **329**, 1188 (2010).

[66]G. Giovannetti, P. A. Khomyakov, G. Brocks, P. J. Kelly, and J. van den Brink, Phys. Rev. B **76**, 073103 (2007).

[67]K. Momma and F. Izumi, J. Appl. Crystallogr. **41**, 653 (2008).